Available online at www.sciencedirect.com
ScienceDirect
Journal of Sound and Vibration 316 (2008) 180–197
JOURNAL OF SOUND AND VIBRATION
www.elsevier.com/locate/jsvi

Dynamic analysis of a lattice structure by homogenization: Experimental validation

Armaghan Salehian[a,*], Daniel J. Inman[b,1]

[a]*Department of Mechanical and Mechatronics Engineering, University of Waterloo, Zoo University Ave. West, Waterloo, ON, Canada N2L 3E1*
[b]*Department of Mechanical Engineering, Virginia Polytechnic Institute and State University, Center for Intelligent Material Systems and Structures, 310 Durham Hall, Mail code 0261, Blacksburg, VA 24061, USA*

Received 6 June 2006; received in revised form 12 February 2008; accepted 18 February 2008
Handling Editor: P. Davies
Available online 8 May 2008

Abstract

A homogenization method is presented for dynamic analysis of truss structures motivated by large satellite applications. The proposed method was previously compared to a full finite element procedure and the experimental verification of the homogenization approach is presented here. Local strains in a planar truss are found in terms of the strain components evaluated at the center of the repeating truss element. Kinetic and strain energy expressions are then derived in terms of the spatial and time derivative of the displacement components at the center of the truss element. Necessary assumptions are made to reduce the order of the strain field of the full model to a geometrically reduced order model. Hamilton's principle is employed to find the governing partial differential equations of motion for the equivalent continuum model. It is shown that the dynamic equations for this structure are similar to those of an anisotropic Timoshenko beam theory. Finally the natural frequencies of the structure are found using the one-dimensional homogenized model. A truss structure was fabricated and tested for the purpose of validation of the developed theory. The results for the frequency response functions and the natural frequencies from the continuum model are shown to be in good agreement with the experiment. As a result, the method shows promise as a tool for use in the analysis and design of lattice structures.

1. Introduction

During the past few years there has been increasing interests for the design of radar satellites to operate in medium Earth orbit (MEO) in order to provide better coverage than low Earth orbit (LEO). Such technology will require fewer satellites for global coverage and thus reduce the overall system costs. A radar antenna operating in MEO has to be so large that it could not launch on existing rockets [1]. Inflatable technology is the solution to this problem. While NASA has flown more missions with mechanically deployed systems so far, inflatable structures can be compressed into far smaller packages and offer a solution not currently

*Corresponding author. Tel.: +1 519 888 4567x38531; fax: +1 519 888 4333.
E-mail addresses: salehian@mme.uwaterloo.ca (A. Salehian), dinman@vt.edu (D.J. Inman).
[1]Tel.: +1 540 231 4709; fax: +1 540 231 2903.

0022-460X/$ - see front matter © 2008 Elsevier Ltd. All rights reserved.
doi:10.1016/j.jsv.2008.02.031

Nomenclature

A_L, A_d	cross-sectional area of longerons and diagonals
$A^{(k)}$	cross-sectional area of member k
$A_{\text{eq.}}$	cross-sectional area of the equivalent continuum model
c	wave speed
d_j	modal participation factor
E_L, E_d	modulus of elasticity of longerons and diagonals
$E^{(k)}$	modulus of elasticity member k
$E_{\text{eq.}}$	modulus of elasticity of the equivalent continuum model
f	frequency (Hz)
I_b	moment of inertia at the boundaries
$I_{\text{eq.}}$	rotary inertia of the cross section of the equivalent continuum model
k	superscript for member k
K	element stiffness matrix
L_L, L_d	length of longerons and diagonal
$L^{(k)}$	length of member k
m_b	mass at the boundaries
m_j	mass of the joints
M	moment
N	longitudinal force
Q	transverse shear force
t	time
T	kinetic energy
T_m	total kinetic energy of the bar members in the truss element
T_e	kinetic energy of the truss element
$T^{(k)}$	kinetic energy of member k
T_j	kinetic energy of the joints
u_1, u_3	displacement components (in x, z directions)
u_1^0, u_3^0	displacement components (in x, z directions) evaluated at the center of the cross section
U_{1j}	mode vector j of the longitudinal vibration
U_{3j}	mode vector j of the bending vibration
U	strain energy
U_e	strain energy of the truss element
$U^{(k)}$	strain energy of member k
$V_{x,i}$, $V_{z,i}$	velocity components of node i of a bar member
x, y, z	Cartesian coordinates
$\alpha_i (i{:}1 \to 6)$	mode shape parameters
ε_x, ε_z, ε_{xz}	strain components evaluated at the center of the cross section
$\varepsilon^{(k)}$	strain in member k
κ_z	curvature component of the cross section
λ	wavelength
ρ_L, ρ_d	density of longerons and diagonals
$\rho^{(k)}$	density of member k
$\rho_{\text{eq.}}$	density of the equivalent continuum model
ψ_0	rotation of the cross section
Ψ_j	mode vector j of the rotational vibration
ω	natural frequencies of the truss in (rad/s)

available using traditional components. Many proposed inflatable designs for space applications consist of truss-like or lattice structures due to their simplicity of construction and large stiffness to mass ratios. Therefore inflatable lattice-type structures are a very suitable solution for space applications and there is primary need for understanding the dynamic behavior of such structures. One such approach is finite element analysis (FEA); however, FEA requires a significant amount of storage capacity and run time to obtain reliable solutions when the number of truss members in the structure is large. Hence, they naturally lead to large order models with limited ability to include damping and may become too large for low-order control law designs. Moreover, many times in dynamic analysis the FEA produces more modes of vibration than are actually needed [2]. Alternatively, the existing methods for control designs for distributed parameter systems can be applied effectively if appropriate continuum model of the structure can be found. Another important advantage of the continuum modeling approach is that a transfer function can easily be obtained between the sensing and actuation points of the structure using the closed form solution [3] which is more desirable than a black box solution for control purposes and can be applied more effectively than FEA. Finally analytical solutions provide better insight into dominant structural physics and behavior and hence can aid in the preliminary design.

Large space structures are too flexible and large to be ground tested. Hence, modeling becomes a key in predicting the structural behavior of such systems. It is possible to ground test the individual components of

these structures in their inflated and rigidized state as previously done in Refs. [4–6]. Once the physical parameters of these components are tested and known, it is desirable to be able to build a model of the truss system made of these components. The method presented here addresses this problem by the proposed homogenization approach. To verify this approach a small-scale metal model of an assembled truss with hinge joint was constructed and tested. This test structure is then used to validate the proposed method. Once validated experimentally as described here and against finite element method as described in Refs. [7,8], the proposed modeling method can be used with confidence for design and control studies.

The following reviews some notable contributions to the analysis of lattice structures. In Refs. [9,10], the local effects are included and the nodal displacements of a truss structure are linearly expanded around their values at the center of the cross section. The reduced order mass and stiffness matrices are derived (a numerical solution); subsequently, the natural frequencies are found. A continuum model for a beam-like lattice truss with rectangular cross-section was developed in Ref. [11] in which the theory of Refs. [9,10] was modified to account for warping of the rectangular cross-section. In some other related work, the continuum models for repetitive beam-like trusses with orthogonal tetrahedral configurations were found [12]. The authors of this work consider an asymmetric configuration in which the axial and shear effects are coupled and the fundamental static and free vibration equations are derived using the constitutive relations and Newton's law. A summary of different approaches on developments of continuum models are reviewed by Ref. [13]. The authors categorize these methods in four different groups: (1) direct methods, (2) discrete field methods, (3) periodic structure approaches, and (4) substitute continuum approaches. In Refs. [14,15] the equivalent stiffness and mass matrices of truss elements with different configurations are found and compared for their stiffness to mass ratios. In another work the governing partial differential equations for a two-dimensional (2-D) lattice structure were derived using the force–displacement relations and Newton's law [16] but no local effects are included which causes inaccuracy for structures with small number of elements. In this model the equivalent stiffness of a truss element is found by applying unit loads in different directions and finding the static deformations. In Ref. [17] the effective elastic and dynamic characteristics for a repeating element are found to derive the reduced FEA mass and stiffness matrices and to find the natural frequencies and mode shapes. The author of a previous work developed a continuum model for large periodic lattice beam using the spectral element approach [18]. His method involves the derivation of the transfer matrices by assembling the spectral element matrices for each structural member within a lattice cell (a numerical solution). The equivalent structural properties for 2-D lattice trusses are presented in that work. The equivalent beam properties in static analysis of beam-like lattice trusses based on the concept of energy equivalence were determined in Ref. [19]. The continuum stresses and strains are defined by their average values over the element. This method is applied to 2-D lattice elements to find the static deflections. It is shown in Ref. [20] that the forces and deformations of a small segment of the truss structure can be related to those of the continuum model to find the anisotropic effective rigidities (stretching, bending, and shearing), and the coupling between them. The local effects in the fundamental truss elements are ignored in the proposed method. In another work, the method of discrete homogenization was employed for continuous modeling of a quasi-repetitive lattice structure [21]. The method consists of assuming an asymptotic series expansion for the node displacements and the tension in truss bar members. The balance equations of nodal displacements and force–displacement relations were developed by the Taylor's expansion of finite differences. The solution is then found by numerical methods for a 2-D truss structure. A complete survey on the two classes of numerical discrete field approaches is provided by Dean and Avent [22]. These approaches are the Micro method, by which one constructs and solves difference equation models (or difference differential equations for mixed discrete–continuous systems), and the Macro method, by which one constructs and solves the summation equation models (or summation integral equations for mixed discrete–continuous systems). In both approaches a set of governing difference equations are obtained and employed to find the continuum model [23–25].

Among all the existing methods for continuum modeling of the structures with repeated patterns very few have been validated experimentally. One such example is the work presented in Ref. [26]. The authors of this work attempt to model a mast as a slender cantilever beam with a tip mass. The effective bending modulus of the structure was obtained using a static load and the resultant deflection. The error for the natural frequencies for this method is up to 92% for the first three bending modes. Presented in Ref. [27] is another work with an

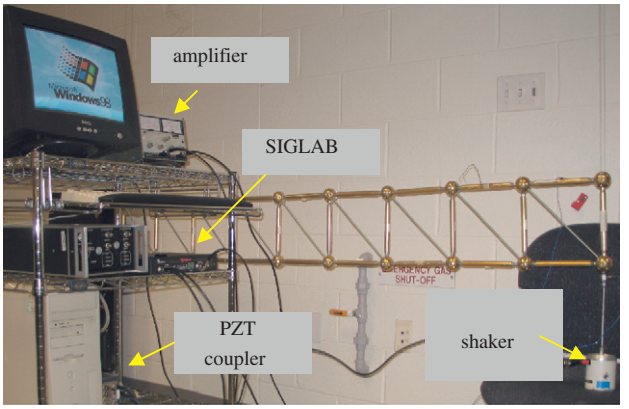

Fig. 1. Photo of the experimental setup.

experimental verification of such approach. However, this work focuses on discussing a method of modeling nonlinearities in the truss joints and the first three frequencies show an error around 10%.

In the current paper, we use a substitute continuum approach based on the energy equivalence concept. We modify the assumptions for the strain and displacement field developed for a three-dimensional (3-D) structure in Refs. [7,8,10] and present them in a form suitable for a planar truss. The local effects for the fundamental truss element (variations of the strain values across the element) are included using a Taylor series expansion as described in Refs. [7,8]. We make the necessary assumptions to solve for the strain components in the 2-D truss in terms of those evaluated at the center of an element which is the same as the strain components of the equivalent one-dimensional (1-D) model. A planar truss was fabricated and the frequency response functions and the natural frequencies are found by an experiment to validate the theory. The results are shown to be in good agreement with the experiment. Additionally the importance of including the masses at the boundaries is shown using an experiment. This boundary condition refers to the part of the elements at the extremes of the structure that cannot be included in the repeating elements. Therefore, the part of these members must be included as a part of the boundary conditions. The latter is also a flaw in all the previous methods. Finally the strain variations are also included in the kinetic energy expressions for the fundamental truss element (also ignored in the previous models). This effect gives us slightly better accuracy for the higher modes of vibration. Finally, the results show higher accuracy than those presented in Refs. [26,27].

2. Modeling

The structure studied in this work is motivated by the Innovative Space Based Radar Antenna Technology program (ISAT).[2] The truss structure presented here is shown in Fig. 1. Here we attempt to find the kinetic and strain energy expressions for the repeating element shown in Fig. 2 as the first step in obtaining a continuum model. The following sections outline the derivation of such expressions in terms of nodal velocities and the strain components. These energy expressions are then written in terms of spatial and time derivatives of the displacement components evaluated at the center of the elements which are the same as those of the equivalent continuum model. Hamilton's principle is then employed to derive the partial differential equations of motion. These equations are then written in the form of an eigenvalue problem and solved to find the frequency response function (FRF) and the natural frequencies of the system.

2.1. Strain energy

A view of the repeating element, the joints and their interconnecting parts are shown in Figs. 2 and 3, respectively. The derivation of the strain energy of the repeating element is outlined in this section. The truss

[2]This program is funded by the Defense Advance Research Project Agency (DARPA).

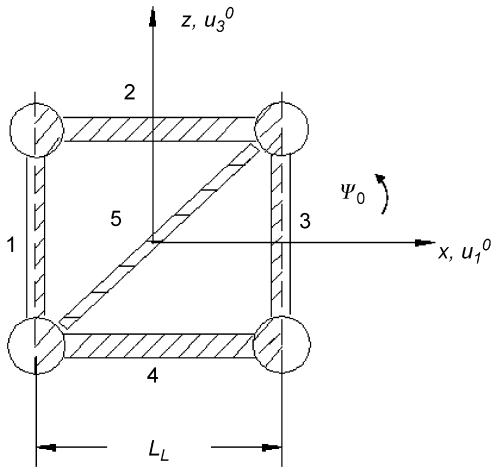

Fig. 2. Schematic of bar members and joints in the truss element.

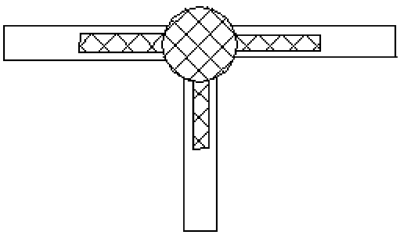

Fig. 3. A view of the joint and the interconnecting parts.

element consists of the shaded area shown in Fig. 2 and the remaining areas belong to the adjacent elements. The members in the truss element are modeled as bars with pin joints. Therefore we assume linear variations for the displacement components (u_1,u_3) along the z-axis and at the center of the cross section of an element. So we get

$$\begin{aligned} u_1(x,y,z) &= u_1^0(x) + z\psi_0(x), \\ u_3(x,y,z) &= u_3^0(x) + z\varepsilon_z(x), \end{aligned} \tag{1}$$

where $u_1(x,y,z)$ and $u_3(x,y,z)$ are the displacement components along the x and z axes shown in Fig. 2 and $u_1^0(x)$, $u_3^0(x)$,and $\psi_0(x)$ are the displacement and rotation components evaluated at the center of the element. The strain component $\varepsilon_z(x)$ is the extensional strain in the z direction evaluated at the center of the element and all of the $u_1^0(x)$, $u_3^0(x)$, $\psi_0(x)$, and $\varepsilon_z(x)$ depend on the x coordinate only. Using Eq. (1) the strain components can be found by taking the derivatives of the displacement field with respect to the coordinates x, y, z,

$$\begin{aligned} \varepsilon_x^{(k)} &= \frac{\partial u_1}{\partial x} = \frac{\partial u_1^0}{\partial x} + z\frac{\partial \psi_0}{\partial x} = \varepsilon_x + z^{(k)}\kappa_z, \\ \varepsilon_z^{(k)} &= \varepsilon_z, \\ \varepsilon_{xz}^{(k)} &= \frac{1}{2}\left(\frac{\partial u_1}{\partial z} + \frac{\partial u_3}{\partial x}\right) = \underbrace{\frac{1}{2}\left(\frac{\partial u_3^0}{\partial x} + \psi_0\right)}_{2\varepsilon_{xz}} = \varepsilon_{xz}, \end{aligned} \tag{2}$$

where superscript k denotes each of the 5 bar members in an element and ε_x, ε_{xz}, ε_z, and κ_z are the strain and the curvature components evaluated at the center of the element and can be written as

$$\varepsilon_x = \frac{\partial u_1^0}{\partial x}, \quad \varepsilon_z = \frac{\partial u_3^0}{\partial z}, \quad \varepsilon_{xz} = \frac{1}{2}\left(\frac{\partial u_3^0}{\partial x} + \psi_0\right), \quad \kappa_z = \frac{\partial \psi_0}{\partial x}. \tag{3}$$

Similar to the assumptions made for a 3-D truss element in Ref. [10], a Taylor series expansion of the strain relations around the coordinate x is then found to account for the strain values at locations with nonzero values of x (points other than the center of the element where $x = 0$). These can be expressed as

$$\begin{aligned}
\varepsilon_x^{(k)} &= \varepsilon_x + z^{(k)}\kappa_z + x^{(k)}\left(\frac{\partial \varepsilon_x}{\partial x} + z^{(k)}\frac{\partial \kappa_z}{\partial x}\right),\\
\varepsilon_z^{(k)} &= \varepsilon_z,\\
\varepsilon_{xz}^{(k)} &= \varepsilon_{xz} + x^{(k)}\left(\frac{\partial \varepsilon_{xz}}{\partial x}\right).
\end{aligned} \tag{4}$$

Members 1–4 shown in Fig. 2 are called the longerons and member 5 is the diagonal member. Using Eqs. (3) and (4) we can expand the strain energy expression of the repeating truss element in terms of the displacement components. A complete derivation is presented in Appendix A. This relation can be written in the following form:

$$\begin{aligned}
U_e = \frac{E_L A_L L_L}{4(E_d A_d L_d + 4E_L A_L L_L)}\Bigg(& 2E_d A_d L_d \psi_0^2 + 2E_d A_d L_d \left(\frac{\partial u_3^0}{\partial x}\right)^2\\
&+ L_L^2 (A_d E_d L_d + 4E_L A_L L_L)\left(\frac{\partial \psi_0}{\partial x}\right)^2 + 4A_d E_d L_d \frac{\partial u_3^0}{\partial x}\frac{\partial u_1^0}{\partial x}\\
&+ 2(3E_d A_d L_d + 8E_L A_L L_L)\left(\frac{\partial u_1^0}{\partial x}\right)^2 + 4E_d A_d L_d \psi_0 \left(\frac{\partial u_3^0}{\partial x} + \frac{\partial u_1^0}{\partial x}\right)\Bigg).
\end{aligned} \tag{5}$$

Here subscripts 'd' and 'L' define the diagonal and the longeron members, respectively.

2.2. Kinetic energy

The next step in obtaining the continuum model is to find the expressions for kinetic energy of the truss element. The kinetic energy of the repeating element can be written in terms of the kinetic energy of the bar members and the joints as

$$T_e = \frac{T^{(1)}}{2} + T^{(2)} + \frac{T^{(3)}}{2} + T^{(4)} + T^{(5)} + T_j, \tag{6}$$

where $T^{(1)}$, $T^{(2)}$, $T^{(3)}$, $T^{(4)}$, and $T^{(5)}$ are the kinetic energy of the bar members and T_j is the kinetic energy of the joints. Note that half of the bar members 1 and 3 belong to the adjacent truss elements; this is considered in the derivation for the kinetic energy of this element. The same assumption was made for the strain energy derivation. A complete derivation for this is shown in Appendix B. Finally, the kinetic energy of the truss element can be expanded in terms of the time derivatives of the displacement components evaluated at the center of the truss element. These displacement components are the same as those of the continuum model, so we get

$$\begin{aligned}
T_e = \frac{1}{2}(3A_L\rho_L L_L + A_d\rho_d L_d)\left(\left(\frac{\partial u_1^0}{\partial t}\right)^2 + \left(\frac{\partial u_3^0}{\partial t}\right)^2\right) + \frac{1}{24}L_L^2(7A_L\rho_L L_L + A_d\rho_d L_d)\left(\frac{\partial \psi_0}{\partial t}\right)^2\\
+ \frac{1}{4}m_j\left(4\left(\frac{\partial u_1^0}{\partial t}\right)^2 + 4\left(\frac{\partial u_3^0}{\partial t}\right)^2 + L_L^2\left(\frac{\partial \psi_0}{\partial t}\right)^2\right).
\end{aligned} \tag{7}$$

2.3. Hamilton's principle and equations of motions

From Eqs. (5) and (7) and using Hamilton's principle, the partial differential equations of motion can be found in the following form:

$$\begin{aligned}
&c_1\left(\psi_0+\frac{\partial u_3^0}{\partial x}+\frac{\partial u_1^0}{\partial x}\right)+c_3\frac{\partial^2\psi_0}{\partial x^2}+c_4\frac{\partial^2\psi_0}{\partial t^2}=0,\\
&c_5\left(\frac{\partial\psi_0}{\partial x}+\frac{\partial^2 u_3^0}{\partial x^2}+\frac{\partial^2 u_1^0}{\partial x^2}\right)+c_2\frac{\partial^2 u_3^0}{\partial t^2}=0,\\
&c_5\left(\frac{\partial^2 u_3^0}{\partial x^2}+\frac{\partial\psi_0}{\partial x}\right)+c_2\frac{\partial^2 u_1^0}{\partial t^2}+c_6\frac{\partial^2 u_1^0}{\partial x^2}=0,
\end{aligned} \tag{8}$$

where

$$\begin{aligned}
c_1&=12A_dE_dL_dA_LE_LL_L,\\
c_2&=(3A_LL_L\rho_L+L_dA_d\rho_d+2m_j)(A_dE_dL_d+4A_LE_LL_L),\\
c_3&=-6L_L^2(A_dE_dL_d+4A_LE_LL_L)A_LE_LL_L,\\
c_4&=L_L^2(7A_LL_L\rho_L+6m_j+L_dA_d\rho_d)(A_dE_dL_d+4A_LE_LL_L),\\
c_5&=-E_dA_dL_dA_LE_LL_L,\\
c_6&=-E_LA_LL_L(3E_dA_dL_d+8E_LA_LL_L).
\end{aligned} \tag{9}$$

The above relation is shown in terms of the displacement components $u_1^0(x)$, $u_3^0(x)$, and ψ_0 (longitudinal, bending, and rotation of the cross section). These are all evaluated at the center of the truss and their derivatives are found along the x coordinate (a 1-D continuum model). The equation shown above is in form to the anisotropic Timoshenko beam model [16]. The conventional Timoshenko beam model was derived for a homogenous isotropic material; a more general form of this theory (orthotropic) shown in Eq. (8) is required for continuum modeling of the truss structure in which all three longitudinal, bending, and rotation of cross section coordinates of vibrations are coupled. Ignoring the longitudinal vibration $u_1^0(x)$ in Eq. (8) results in a conventional Timoshenko beam model.

2.4. Boundary conditions

The fundamental repeating truss element consists of the shaded area shown in Fig. 2 and the remaining parts in the figure belong to the adjacent elements. By assembling this element along the length of the structure there will be additional parts at the two ends of the truss which do not belong to any of the elements. Hence they become part of the boundary conditions for the truss. These boundary conditions for the structure can be expressed in the following form:

at $x=0$:

$$N(x,t)=m_b\frac{\partial^2 u_1^0(x,t)}{\partial t^2},\quad Q(x,t)=m_b\frac{\partial^2 u_3^0(x,t)}{\partial t^2},\quad M(x,t)=I_b\frac{\partial^2\psi_0(x,t)}{\partial t^2}, \tag{10a}$$

at $x=L$:

$$N(x,t)=-m_b\frac{\partial^2 u_1^0(x,t)}{\partial t^2},\quad Q(x,t)=-m_b\frac{\partial^2 u_3^0(x,t)}{\partial t^2},\quad M(x,t)=-I_b\frac{\partial^2\psi_0(x,t)}{\partial t^2}, \tag{10b}$$

where m_b and I_b are the mass and rotary inertia at the boundaries. Failure to include these at the boundary represents a flaw in all the previously published methods. Fig. 9 depicts a comparison between the frequency response function without including the boundary conditions and the experiment. The figure clearly shows the non-negligible difference between the theory and the experiment. To include the effect of the boundaries, the stiffness matrix of the element must be found; this is easily accomplished with Eq. (5). With the stiffness matrix the longitudinal force N, transverse shear force Q, and the moment at the cross section M can be written in the

terms of the displacement components in the following form:

$$\begin{bmatrix} N \\ Q \\ M \end{bmatrix} = \underbrace{\begin{bmatrix} \frac{A_L E_L L_L (3A_d E_d L_d + 8A_L E_L L_L)}{(A_d E_d L_d + 4A_L E_L L_L)} & \frac{A_L E_L L_L A_d E_d L_d}{(A_d E_d L_d + 4A_L E_L L_L)} & 0 \\ \frac{A_L E_L L_L A_d E_d L_d}{(A_d E_d L_d + 4A_L E_L L_L)} & \frac{A_L E_L L_L A_d E_d L_d}{(A_d E_d L_d + 4A_L E_L L_L)} & 0 \\ 0 & 0 & \frac{A_L E_L L_L (L_L^2 (A_d E_d L_d + 4A_L E_L L_L))}{2(A_d E_d L_d + 4A_L E_L L_L)} \end{bmatrix}}_{K} \begin{bmatrix} \frac{\partial u_1^0}{\partial x} \\ \psi_0 + \frac{\partial u_3^0}{\partial x} \\ \frac{\partial \psi_0}{\partial x} \end{bmatrix}. \tag{11}$$

Appendix C shows a complete solution for the governing partial differential equations of motion and the boundary conditions. Having Eq. (C.5) and the solutions for the mode shape parameters α_j from Eq. (C.3), the time response in Eq. (C.6) can be expanded in terms of frequencies ω and the modal participation factors d_j. Additionally, the boundary conditions in Eqs. (10) and the constitutive Eq. (11) gives us a relation in terms the displacement components and their spatial and time derivatives evaluated at the two ends of the truss (boundary conditions). A combination of all these results in six linear algebraic equations that define the boundary conditions for this structure and can be written in the form:

$$[g(\omega)]\{d_j\} = 0. \tag{12}$$

To get a nontrivial solution it must be true that

$$|g(\omega)| = 0. \tag{13}$$

Finally, the solution of the above equation provides the natural frequencies of the structure.

2.5. Wavelengths and frequencies

The natural frequencies from this model are compared with the values of an experiment as shown in the following sections. It is also interesting to examine the error in the frequency estimations with respect to the wavelengths. As previously mentioned, Eq. (8) is similar to the governing equations of motion of an anisotropic Timoshenko beam. Therefore, from the coefficients in Eq. (9) we can find the material and geometrical properties of the equivalent continuum model, the result is

$$\frac{E_{\text{eq.}} I_{\text{eq.}}}{\rho_{\text{eq.}} A_{\text{eq.}}} = \frac{L_L^2 A_L E_L L_L}{2(3A_L L_L \rho_L + 2m_j + L_d A_d \rho_d)}. \tag{14}$$

From the dispersion relation for the phase velocity of the bending waves we have

$$c = \sqrt[4]{\frac{E_{\text{eq.}} I_{\text{eq.}}}{\rho_{\text{eq.}} A_{\text{eq.}}}} \sqrt{\omega} \Rightarrow c = \sqrt[4]{\frac{L_L^2 A_L E_L L_L}{2(3A_L L_L \rho_L + 2m_j + L_d A_d \rho_d)}} \sqrt{\omega}. \tag{15}$$

Therefore, the wavelength for each frequency component is of the form of

$$\lambda = \sqrt[4]{\frac{L_L^2 A_L E_L L_L}{2(3A_L L_L \rho_L + 2m_j + L_d A_d \rho_d)}} \sqrt{\frac{2\pi}{f}}, \tag{16}$$

where f is the frequency in (Hz).

2.6. Effects of including the strain components in the kinetic energy of the repeating element

A complete derivation of the kinetic energy of the element is presented in Appendix B. As mentioned in the appendix the strain values are ignored in this derivation, similar to Refs. [7,8,10]. Presented here is a

modification of this method. For the case that the strain variations are included in the expression for the kinetic energy of the fundamental truss element, we get

$$T_e = \frac{1}{2}(3A_L\rho_L L_L + A_d\rho_d L_d + 2m_j)\left(\left(\frac{\partial u_1^0}{\partial t}\right)^2 + \left(\frac{\partial u_3^0}{\partial t}\right)^2\right) + \frac{1}{24}L_L^2(7A_L\rho_L L_L + A_d\rho_d L_d + 6m_j)\left(\frac{\partial \psi_0}{\partial t}\right)^2 + \frac{(A_dE_dL_LL_d)^2}{24(A_dE_dL_d + 4A_LE_LL_L)^2}(7A_L\rho_L L_L + A_d\rho_d L_d + 6m_j)\left(\left(\frac{\partial^2 u_1^0}{\partial x\partial t}\right) + \left(\frac{\partial^2 u_3^0}{\partial x\partial t}\right) + \left(\frac{\partial \psi_0}{\partial t}\right)\right)^2. \quad (17)$$

Using Hamilton's principle, the equations of motion for the system can be found as follows:

$$\begin{aligned}
&c_1\left(\psi_0 + \frac{\partial u_3^0}{\partial x} + \frac{\partial u_1^0}{\partial x}\right) + c_3\frac{\partial^2\psi_0}{\partial x^2} + c_4\frac{\partial^2\psi_0}{\partial t^2} + c_7\left(\frac{\partial^3 u_3^0}{\partial x\partial t^2} + \frac{\partial^3 u_1^0}{\partial x\partial t^2} + \frac{\partial^2\psi_0}{\partial^2 t}\right) = 0,\\
&12c_5\left(\frac{\partial\psi_0}{\partial x} + \frac{\partial^2 u_3^0}{\partial x^2} + \frac{\partial^2 u_1^0}{\partial x^2}\right) + 12c_2\frac{\partial^2 u_3^0}{\partial t^2} - c_7\left(\frac{\partial^4 u_3^0}{\partial x^2\partial t^2} + \frac{\partial^4 u_1^0}{\partial x^2\partial t^2} + \frac{\partial^3\psi_0}{\partial x\partial^2 t}\right) = 0,\\
&12c_5\left(\frac{\partial^2 u_3^0}{\partial x^2} + \frac{\partial\psi_0}{\partial x}\right) + 12c_2\frac{\partial^2 u_1^0}{\partial t^2} + 12c_6\frac{\partial^2 u_1^0}{\partial x^2} - c_7\left(\frac{\partial^4 u_3^0}{\partial x^2\partial t^2} + \frac{\partial^4 u_1^0}{\partial x^2\partial t^2} + \frac{\partial^3\psi_0}{\partial x\partial^2 t}\right) = 0,
\end{aligned} \quad (18)$$

where the coefficients c_1–c_6 are given by Eq. (9). The coefficient c_7 is

$$c_7 = \frac{(E_dA_dL_dL_L)^2}{(E_dA_dL_d + 4E_LA_LL_L)}(7A_LL_L\rho_L + \rho_dA_dL_d + 6m_j). \quad (19)$$

Finding the solution for these partial differential equations results in the natural frequencies of the system. These frequencies are presented in Table 4. The results are slightly more accurate when compared to the previous case where all the strain components are ignored in the kinetic energy derivations. This is particularly more noticeable for the last frequency shown in the table.

3. Experimental setup

Our goal here is to construct and test a 2-D laboratory truss to provide some element of validation for the concept of the homogenization method presented here and in Refs. [7,8]. The structure consists of 9 truss elements shown in Fig. 2. Each truss element is made of tubular bars and joints as illustrated in Figs. 2 and 3. The longerons members are made of aluminum tubes and the diagonals are made of steel rods. Threaded aluminum ball joints, shown in Fig. 3, are used to connect the bar members. Fig. 4 depicts a schematic of the experiment with sensor and actuator locations. The truss structure was hung on wires from the ceiling at its ends. The truss dimensions are 1960 mm × 217.6 mm. Other structural properties such as density and modulus of longerons and diagonals are provided in Tables 1 and 2.

To validate the results of the continuum model, the natural frequencies and the frequency response functions were obtained experimentally. Fig. 1 shows a photo of the experimental setup. The setup includes the truss structure, a Windows 98 PC with Matlab 6.0, a Piezotron coupler model Kistler 5122, a SIGLAB unit 20-42 DSP data acquisition Board (V3.2), an accelerometer (PCB PIEZOTRONICS Model 352C22) with a sensitivity of 1 mV/(m/s^2), a shaker, a high voltage amplifier model TREK 50/750 and a force transducer model 208 A SN 841 with a sensitivity of 112.410 V/KN. A chirp signal of the frequency range of 1–500 (Hz) is used as an input excitation to this structure. This signal is provided by the SIGLAB unit which is fed to the shaker after passing through the amplifier. The resultant input force to the structure is then measured by the force transducer which is attached to the shaker. The accelerometer is used to measure the acceleration of measurement points in the truss. The PZT sensor in the accelerometer and the force transducer produce a charge and the impedance converter in these elements convert this charge to a voltage signal that can easily be measured. On the other hand the impedance converter requires a voltage and a current to operate. The Piezotron coupler is used to supply this current and voltage to the accelerometer and the force transducer. The data collected by the accelerometer and the force transducer was fed into the SigLab DSP Board which is a signal-processing plug-in compatible with MATLAB. Finally the ratio of the force and acceleration gives us

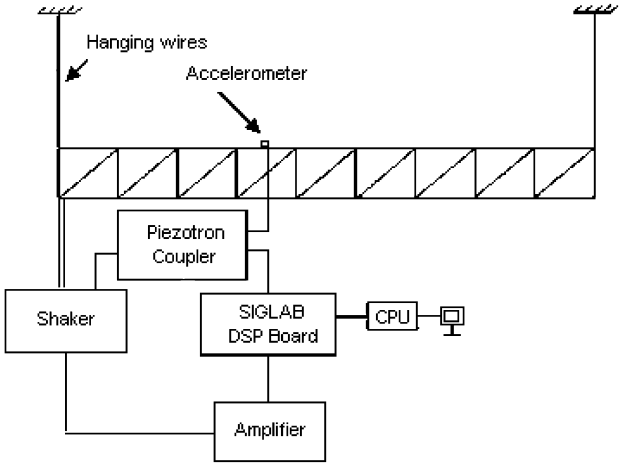

Fig. 4. Schematic of the experimental setup.

Table 1
Material and geometrical properties of the bar members

Member	Cross sectional area (m^2)	Modulus (N/m^2)	Density (kg/m^3)	Length (m)
Longerons/battens	7.129×10^{-5}	6.8948×10^{10}	2416	217.6×10^{-3}
Diagonal	2.107×10^{-5}	2×10^{11}	7850	254.0×10^{-3}

Table 2
Properties of the truss

Total length of truss (m)	Number of truss elements	Mass of the ball joint (kg)	Structure weight (kg)	Mass at the boundary (kg)	Rotary inertia at the boundary ($kg\,m^2$)
1.96	9	0.1927	4.836	0.1392	0.0016

the frequency response functions for the measurement points. ME'scopeVES (Visual Engineering Series) version 4.0 by Vibrant Technology Inc. is employed to plot the experimental mode shapes. An animation snapshot of the experimental mode shapes are presented in Fig. 6.

4. Numerical results

The experimental natural frequencies are found using the peak–peak method presented in Ref. [29] and the results for the theory and the experiment are presented in Tables 3 and 4. The errors in the estimation of the first 4 natural frequencies (0–500 Hz) are 0.07%, 0.65%, 1.57%, and 9.2%, respectively. Fig. 5 shows the frequency response function, coherence, and the phase plots from the experiment. Since the strings at the boundaries have a finite stiffness, the structure has a very small fundamental frequency around 7 Hz which is related to the rigid body mode of the truss. The second, third, and the fourth natural frequencies are also shown in the figure. The two modes shown in the figure around the 250 Hz are related to the out-of-plane torsional modes, which are not estimated by the theory. Because we model the structure as a truss there would be no stiffness in the out-of-plane motion due to the hinge connections: i.e., the structure can fold but not bend in that direction. The fact that these are the torsional modes has been tested by looking at the imaginary parts

Table 3
Theoretical and experimental natural frequencies

Mode	Theoretical frequency (Hz)	Experimental frequency (Hz)	Error (%)
1	6.88	6.875	0.07
2	154	153	0.65
3	319	324	1.57
4	491	444	9.57

Table 4
Theoretical and experimental natural frequencies (strain components included in the kinetic energy terms)

Mode	Theoretical frequency (Hz)	Experimental frequency (Hz)	Error (%)
1	6.88	$\approx$6.875	0.07
2	154	153	0.65
3	319	324	1.57
4	489	444	9.20

of the frequency response functions shown in Fig. 5b. As shown in this figure the imaginary part of the frequency response functions around 250 Hz is very small. This clearly shows that the peaks around this frequency are related to the out-of-plane modes which are measured in a direction different from the accelerometer measurements. Therefore the accelerometer does not completely capture these peaks. Also, to assure these are the torsional modes and the peak around the 324 Hz is the second bending mode, the experimental mode shapes are presented in Fig. 6. These are the snapshots for the mode shapes animations, which are found using the ME'scopeVES software. As demonstrated in these figures the mode shape around the frequency of 324 Hz has clearly the form of the second bending mode shape. This proves that neither of the two small peaks around the 250 Hz can be the second mode. Fig. 7 shows a comparison between the theoretical frequency response functions plots with and without including the effects of the strings at the boundaries. From the figure, this effect is more noticeable and needs to be included for the lower frequencies. However, the higher frequencies (i.e., the first, second, and the third vibration modes) change insignificantly in this model. This is because the rigid body mode in this structure is well separated from the vibrational modes. To account for the effect of the strings we consider that the mass of the truss is held by wires with very small stiffness (a single degree of freedom model) which results in a very small natural frequency for the equivalent mass-stiffness system (truss and the strings). This frequency has a very small value ($\approx$7 Hz) which is clearly shown in the figure. Fig. 8 shows a comparison between the frequency response functions plots for the experiment and the theory for the case that the effects of the strings at the boundary conditions are not included. It is also clear from this figure that this effect needs to be included to obtain results in better agreement with the experiment. A comparison between the frequency response functions from the theory and experiment when no mass and no strings are included at the boundaries (free–free) are presented in Fig. 9. As shown, ignoring the mass at the boundaries results in a significant discrepancy between the theory and experiment which indicates the importance of including the boundary conditions in the form presented in Section 2.4 (a flaw of the previously published methods).

In reference to Fig. 5d, the coherence values are excellent for this experiment, especially around the peaks (natural frequencies). There is a significant drop in the value of the coherence around the anti-resonance frequency which is expected due to a zero response in that region. Fig. 10 provides an enlarged view of the coherence around the 4th natural frequency. An approximate value of 99% is obtained around this peak.

Fig. 11 shows the error of the frequency estimations with respect to the wavelengths that is higher for smaller wavelengths. This is because the error is dependent upon the ratio of the element span to the wavelength. When the wavelength spans larger number of elements the estimations are more accurate.

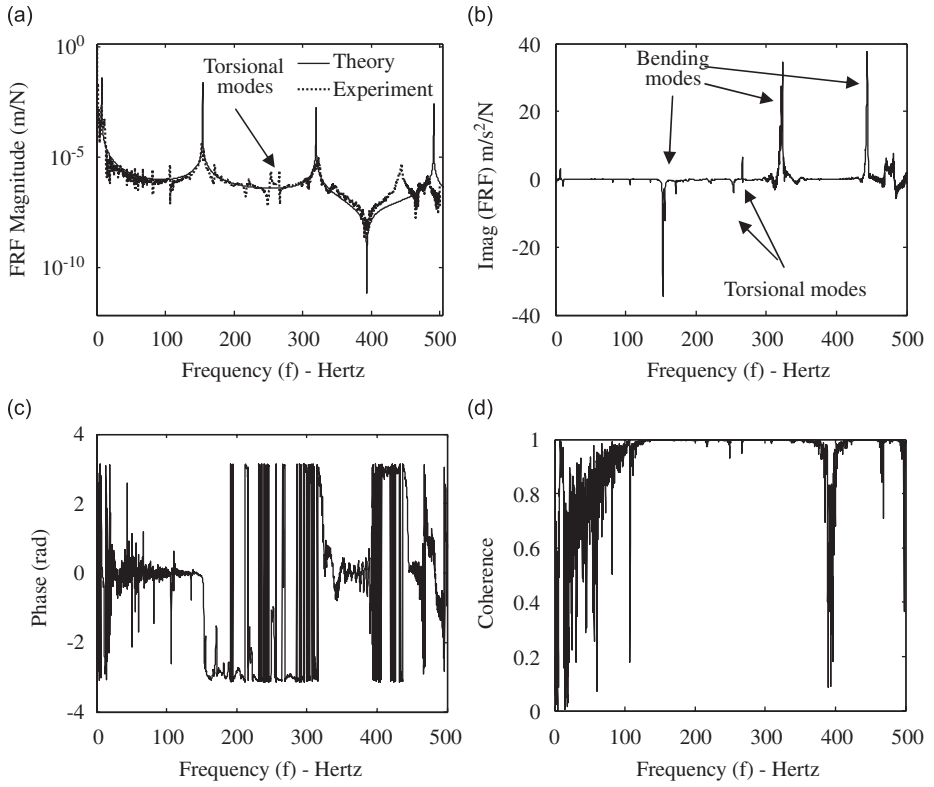

Fig. 5. Frequency domain results: (a) experimental and theoretical FRF magnitude plots, (b) imaginary part of the FRF, (c) phase plot, and (d) coherence plot.

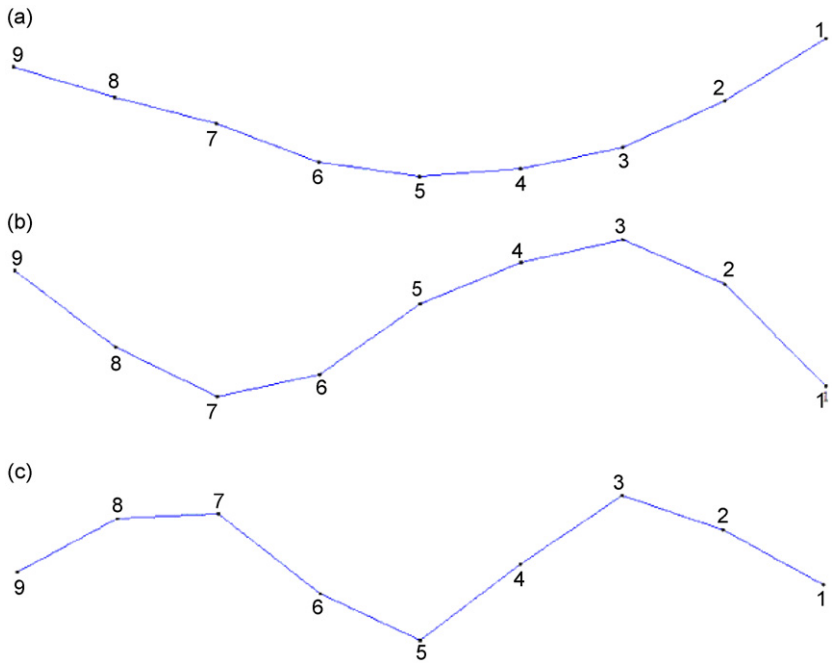

Fig. 6. Snapshots of experimental mode shapes: (a) first mode shape at 153 Hz, (b) second mode shape at 324 Hz, and (c) third mode shape at 444 Hz.

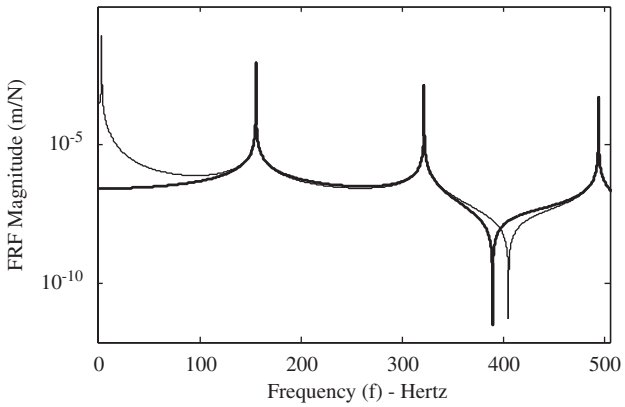

Fig. 7. Theoretical frequency response functions for the lattice with strings attached (thinner line) and without strings (thicker line).

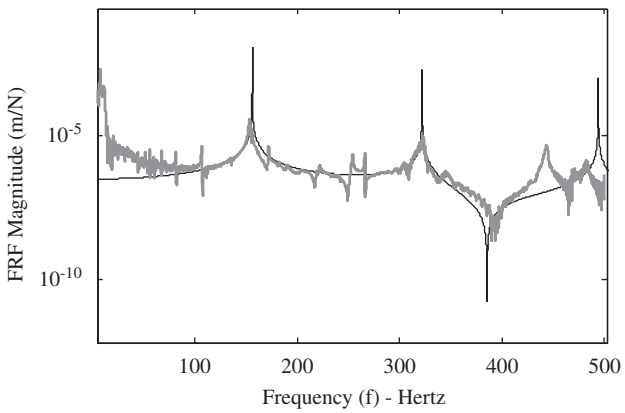

Fig. 8. Theoretical frequency response function without strings (thinner line), experiment (thicker line).

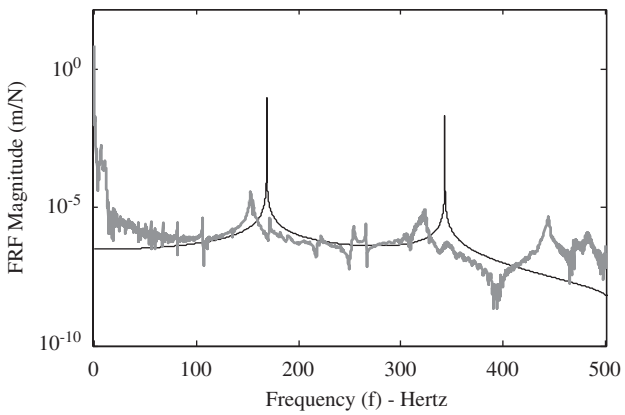

Fig. 9. Theoretical frequency response function with no mass and no string at the boundaries (thinner line) and experiment (thicker line) and theory (thinner line).

Likewise for the wavelengths smaller than the size of the truss element the accuracy of the estimations cannot be considered accurate. For the fundamental frequency the wavelength is 3 m and for the 4th natural frequency it is approximately 1.7 m that spans only 8 elements.

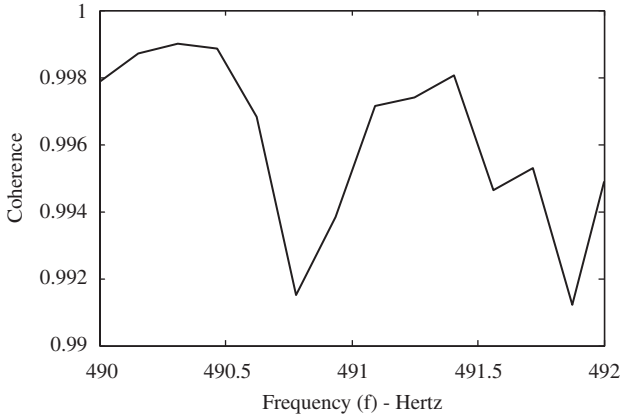

Fig. 10. Coherence values around the 4th natural frequency.

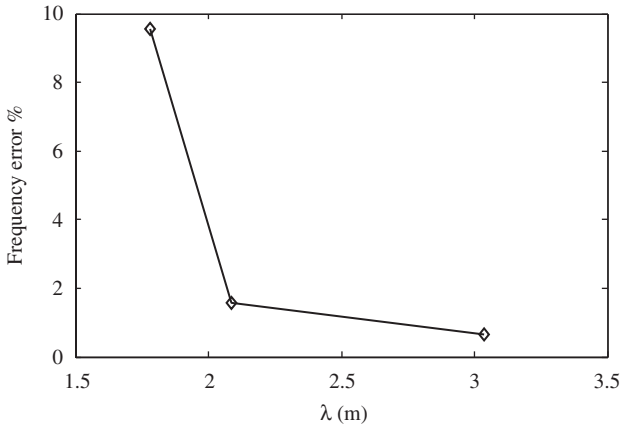

Fig. 11. Error of the frequency estimations with respect to wavelengths.

5. Conclusion

Due to the large size and flexibility of the large space structures, they cannot be tested under the laboratory conditions. Also, these structures behave differently under such conditions compared to the actual space conditions. Therefore accurate modeling is a key issue in understanding the dynamics and control of such structures. One such approach is to derive low-order accurate homogenized models. This method has several advantages, for example, homogenization techniques result in systems with fewer degrees of freedom and hence we have simpler models compared to the FEA, which usually produces more number of modes than actually needed. Also, the existing control law designs for distributed parameter models can effectively be used for continuum models. Presented here are a homogenized model and the experimental validation of the model for a planar truss. It is shown that the continuum model found has the form similar to an anisotropic Timoshenko beam. The governing partial differential equation consists of 3 coupled equations of motion which are the longitudinal, bending, and rotation of the cross section. The natural frequencies and the frequency response functions of the system are found for this model. Such results are validated against the experimental values and they are shown to be in good agreement.

Acknowledgments

This research was conducted at the Center for Intelligent Materials Systems and Structures (CIMSS) at Virginia Polytechnic Institute and State University. This work was supported by the Defense Advanced

Research Projects Agency (DARPA) through NASA-LaRc and the National Institute of Aerospace (NIA), for which we are grateful.

Appendix A. Strain energy derivation

The strain energy of a bar in tension or compression can be written as

$$U^{(k)} = \tfrac{1}{2}E^{(k)}A^{(k)}L^{(k)}(\varepsilon^{(k)})^2, \tag{A.1}$$

where $\varepsilon^{(k)}$ is the strain value along the bar and can be found using the directional cosines between the bar member and the strain components shown in Eq. (4). Using Eq. (A.1) the strain energy of the truss element can be found

$$U_e = \frac{1}{2}E_L A_L L_L\left((\varepsilon_x^{(2)})^2 + (\varepsilon_x^{(4)})^2 + \frac{(\varepsilon_z^{(1)})^2 + (\varepsilon_z^{(3)})^2}{2}\right) + \frac{1}{2}E_d A_d L_d\left(\frac{(\varepsilon_x^{(5)})}{2} + (\varepsilon_{xz}^{(5)}) + \frac{(\varepsilon_z^{(5)})}{2}\right)^2. \tag{A.2}$$

From the strain components in Eqs. (4) and (A.2) the strain energy of an element can be written in terms of the strain components at the center which is the key in deriving the continuum model. So we get

$$U_e = \tfrac{1}{8}(E_d A_d L_d(\varepsilon_x + \varepsilon_z + 2\varepsilon_{xz})^2 + 2E_L A_L L_L(4\varepsilon_x^2 + 2\varepsilon_z^2 + L_L^2\kappa_z^2)). \tag{A.3}$$

Finally using Eqs. (3) and (A.3) the strain energy can be written in terms of the spatial derivatives of the displacement components.

To obtain an equivalent 1-D model the strain energy needs to be expanded in terms of the displacement components evaluated at the center and their derivative values with respect to the x-axis *only*. Therefore the strain component ε_z in Eq. (3) needs to be found in terms of the other strain components. Similar to the approach used in Refs. [7,8], we use the following relation to solve for ε_z:

$$\frac{\partial U_e}{\partial \varepsilon_z} = 0. \tag{A.4}$$

Using Eqs. (A.4) and (A.4) we find the following:

$$E_L A_L L_L \varepsilon_z + \tfrac{1}{4}E_d A_d L_d(\varepsilon_x + \varepsilon_z + 2\varepsilon_{xz}) = 0. \tag{A.5}$$

A solution to Eq. (A.5) results in the following relation for ε_z:

$$\varepsilon_z = -\frac{A_d E_d L_d(\varepsilon_x + 2\varepsilon_{xz})}{A_d E_d L_d + 4E_L A_L L_L}. \tag{A.6}$$

Eqs. (A.6) and (A.3) gives us the relation for the strain energy of the element in terms of the strain components and their derivative along the coordinate x. These are the same as the equivalent 1-D continuum model:

$$\begin{aligned} U = \frac{1}{4(E_d A_d L_d + 4E_L A_L L_L)}&(E_L A_L L_L(2(3E_d A_d L_d + 8E_L A_L L_L)\varepsilon_x^2 + 8E_d A_d L_d \varepsilon_x \varepsilon_{xz} \\ &+ 8E_d A_d L_d \varepsilon_{xz}^2 + L_L^2(E_d A_d L_d + 4E_L A_L L_L)\kappa_z^2)). \end{aligned} \tag{A.7}$$

Appendix B. Kinetic energy derivation

It can be proved very easily that the kinetic energy of a bar element shown in Fig. B.1 can be written as

$$T = \tfrac{1}{6}\rho AL(V_{x,1}^2 + V_{z,1}^2 + V_{x,2}^2 + V_{z,2}^2 + V_{x,1}V_{x,2} + V_{z,1}V_{z,2}), \tag{B.1}$$

where ρ, A, L are density, cross-sectional area and length of the bar and the nodal velocity components are shown in Fig. B.1. Using Eqs. (B.1) and (1) and ignoring the stain terms in the kinetic energy derivations (the

effect of including this is shown in Section 2.6), we get the following relation for the kinetic energy of the bar member (k):

$$T^{(k)} = \frac{1}{6}\rho^{(k)}A^{(k)}L^{(k)}\left(\left(\frac{\partial u_1^0}{\partial t} + z_{(1)}^{(k)}\frac{\partial \psi_0}{\partial t}\right)^2 + 3\left(\frac{\partial u_3^0}{\partial t}\right)^2 + \left(\frac{\partial u_1^0}{\partial t} + z_{(2)}^{(k)}\frac{\partial \psi_0}{\partial t}\right)^2 + \left(\frac{\partial u_1^0}{\partial t} + z_{(1)}^{(k)}\frac{\partial \psi_0}{\partial t}\right)\left(\frac{\partial u_1^0}{\partial t} + z_{(2)}^{(k)}\frac{\partial \psi_0}{\partial t}\right)\right). \tag{B.2}$$

Here $z_{(1)}^{(k)}$ and $z_{(2)}^{(k)}$ are the z coordinate of each of the two nodes of the bar member (k). Also for the joints we get

$$T_j = m_j\left(\left(\frac{\partial u_1^0}{\partial t}\right)^2 + \left(\frac{\partial u_3^0}{\partial t}\right)^2 + \frac{1}{4}L_L^2\left(\frac{\partial \psi_0}{\partial t}\right)^2\right). \tag{B.3}$$

Using Eq. (B.2) the kinetic energy for the truss element (with no joints) can be expanded in the following form:

$$T_m = \sum_{k=1}^{5} T^{(k)} = \frac{1}{2}(3A_L\rho_L L_L + A_d\rho_d L_d)\left(\left(\frac{\partial u_1^0}{\partial t}\right)^2 + \left(\frac{\partial u_3^0}{\partial t}\right)^2\right) + \frac{1}{24}L_L^2(7A_L\rho_L L_L + A_d\rho_d L_d)\left(\frac{\partial \psi_0}{\partial t}\right)^2. \tag{B.4}$$

Using Eqs. (B.4) and (B.3) we get the relation for the kinetic energy of the truss element as follows:

$$T_e = T_m + T_j. \tag{B.5}$$

Appendix C. Partial differential equation solution

Using a similar approach by Doyle [28] the solution of the PDE in Eq. (9) can be found. Making the assumption of a harmonic solution, we get

$$\left.\begin{aligned} u_1^0 &= U_1 e^{\alpha x} e^{i\omega t} \\ u_3^0 &= U_3 e^{\alpha x} e^{i\omega t} \\ \psi_0 &= \Psi e^{\alpha x} e^{i\omega t} \end{aligned}\right\} \Rightarrow \begin{Bmatrix} u_1^0 \\ u_3^0 \\ \psi_0 \end{Bmatrix} = \begin{Bmatrix} U_1 \\ U_3 \\ \Psi \end{Bmatrix} e^{\alpha x} e^{i\omega t}, \tag{C.1}$$

where U_1, U_3, and ψ are the amplitudes of vibration along different coordinates, α is the mode shape parameter and ω is the natural frequency. Substituting Eq. (C.1) in Eq. (8) we get the following

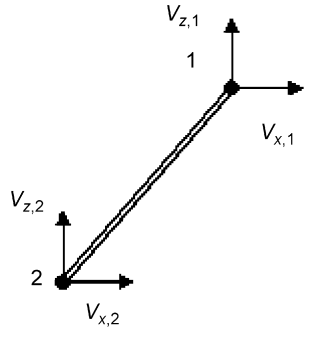

Fig. B1. Schematic view of a bar and the nodal velocities.

eigenvalue problem:

$$\underbrace{\begin{bmatrix} c_1\alpha & c_1\alpha & c_1+c_3\alpha^2-c_4\omega^2 \\ c_5\alpha^2 & c_5\alpha^2-c_2\omega^2 & c_5\alpha \\ -c_2\omega^2+c_6\alpha^2 & c_5\alpha^2 & c_5\alpha \end{bmatrix}}_{H} \begin{Bmatrix} U_1 \\ U_3 \\ \Psi \end{Bmatrix} = 0. \tag{C.2}$$

To obtain a nontrivial solution the determinant of matrix H should vanish. So the following should hold:

$$\mathrm{Det}(H) = 0 \Rightarrow a_1\alpha^6 + a_2\alpha^4 + a_3\alpha^2 + a_4 = 0, \tag{C.3}$$

where

$$\begin{aligned} a_1 &= c_3c_5^2 - c_3c_5c_6, \\ a_2 &= c_2c_3c_5\omega^2 - c_4c_5^2\omega^2 + c_2c_3c_6\omega^2 + c_4c_5c_6\omega^2, \\ a_3 &= -c_1c_2c_5\omega^2 + c_1c_2c_6\omega^2 - c_2^2c_3\omega^4 - c_2c_4c_5\omega^4 - c_2c_4c_6\omega^4, \\ a_4 &= -c_1c_2^2\omega^4 + c_2^2c_4\omega^6. \end{aligned} \tag{C.4}$$

Eq. (C.3) is a cubic polynomial in terms of α^2 and the solutions for α are the roots of this polynomial which appear as complex conjugates. For each of the 6 roots of α_j the solution of the mode vectors can be expressed in the following form:

$$\begin{aligned} U_{1j} &= \begin{vmatrix} c_1\alpha_j & c_1+c_3\alpha_j^2-c_4\omega^2 \\ c_5\alpha_j^2-c_2\omega^2 & c_5\alpha_j \end{vmatrix} = -c_3c_5\alpha_j^4 + c_1c_2\omega^2 + c_2c_3\alpha_j^2\omega^2 + c_4c_5\alpha_j^2\omega^2 - c_2c_4\omega^4, \\ U_{3j} &= -\begin{vmatrix} c_1\alpha_j & c_1+c_3\alpha_j^2-c_4\omega^2 \\ \alpha_j^2c_5 & c_5\alpha_j \end{vmatrix} = c_3c_5\alpha_j^4 - c_4c_5\alpha_j^2\omega^2, \\ \Psi_j &= \begin{vmatrix} \alpha_jc_1 & \alpha_jc_1 \\ \alpha_j^2c_5 & \alpha_j^2c_5-c_2\omega^2 \end{vmatrix} = -c_1c_2\alpha_j\omega^2. \end{aligned} \tag{C.5}$$

Here subscript j denotes each of the 6 roots $\alpha_j(j{:}1\to6)$ for a frequency ω. Finally the free vibration solution can be expanded in terms of the mode vectors, mode shape parameters (α_j) and natural frequencies, ω, as follows:

$$\begin{Bmatrix} u_1^0(x,t) \\ u_3^0(x,t) \\ \psi_0(x,t) \end{Bmatrix} = \sum_{j=1}^{6} d_j \begin{Bmatrix} U_{1j} \\ U_{3j} \\ \Psi_j \end{Bmatrix} \mathrm{e}^{\alpha_j x}\mathrm{e}^{\mathrm{i}\omega t}, \tag{C.6}$$

where coefficients d ($j{:}1\to6$) are the modal participation factors of the mode shape parameters α_j for each frequency ω and can be found from the boundary conditions as shown in Section 2.4.

References

[1] A.B. Chmielewski, Overview of Gossamer structures, in: C.H.M. Jenkins (Ed.), *Gossamer Spacecraft: Membrane and Inflatable Structures Technology for Space Applications, Progress in Astronautics and Aeronautics*, Vol. 191, AIAA, Reston, VA, 2001, pp. 2–3.

[2] C.T. Sun, S.W. Liebbe, Global-local approach to solving vibration of large truss structures, *AIAA Journal* 28 (2) (1990) 303–308.

[3] B. Yang, C.A. Tan, Transfer functions of one-dimensional distributed parameter systems, *ASME Journal of Applied Mechanics* 59 (4) (1992) 1009–1014.

[4] P.A. Tarazaga, D.J. Inman, W.K. Wilkie, Control of space rigidizable inflatable boom using macro-fiber composite, *Journal of Vibration and Control* 13 (7) (2007) 935–950.

[5] R.S. Papa, J.O. Lassiter, B.P. Ross, Structural dynamics experimental activities in ultralightweight and inflatable space structures, *AIAA Journal of Spacecraft and Rockets* 40 (1) (2003) 15–23.

[6] K. Guidanean, G.T. Williams, An inflatable rigidizable truss structure with complex joints, *Proceedings of the AIAA/ASME/SAE 39th Structures, Structural Dynamics and Materials Conference*, Long Beach, CA, 1998, pp. 2797–2806.

[7] A. Salehian, T.M. Seigler, D.J. Inman, Dynamic effects of a radar panel mounted on a truss satellite, *AIAA Journal* 45 (7) (2007) 1642–1654.
[8] A. Salehian, E.M. Cliff, D.J. Inman, Continuum modeling of an innovative space based radar antenna truss, *American Society of Civil Engineers Journal of Aerospace, Festschrift Issue* 19 (4) (2006) 227–240.
[9] A.K. Noor, W.H. Greene, M.S. Anderson, Continuum models for static and dynamic analysis of repetitive lattices, *Proceedings of the AIAA/ASME/SAE 18th Structures, Structural Dynamics and Materials Conference*, San Diego, California, 1977, pp. 299–310.
[10] A.K. Noor, M.S. Anderson, W.H. Greene, Continuum models for beam and plate-like lattice structures, *AIAA Journal* 16 (12) (1978) 1219–1228.
[11] A.K. Noor, C.M. Andersen, Analysis of beamlike lattice trusses, *Computer Methods in Applied Mechanics and Engineering* 20 (1) (1979) 53–70.
[12] A.K. Noor, W.C. Russell, Anisotropic continuum models for beamlike lattice trusses, *Computer Methods in Applied Mechanics and Engineering* 57 (3) (1986) 257–277.
[13] A.K. Noor, Continuum modeling for repetitive lattice structures, *Applied Mechanics Review* 41 (7) (1988) 285–296.
[14] A.H. Nayfeh, M.S. Hefzy, Continuum modeling of three dimensional rod-like discrete structures, *Proceedings of the International Symposium on Continuum Models of Discrete Systems*, University of Waterloo, Waterloo, Canada, 1977, pp. 339–357.
[15] M.S. Lake, E.C. Kalng, Generation and comparison of globally isotropic space-filling truss structures, *AIAA Journal* 30 (5) (1992) 1416–1424.
[16] C.T. Sun, B.J. Kim, Continuum modeling of periodic truss structures, in: N. Stubbs, D. Krajcinovic (Eds.), *Damage Mechanics and Continuum modeling*, American Society of Civil Engineers, New York, 1985, pp. 57–71.
[17] U. Lee, Dynamic continuum plate representations of large thin lattice structures, *AIAA Journal* 31 (9) (1993) 1734–1736.
[18] U. Lee, Equivalent continuum representation of lattice beams: spectral element approach, *Engineering Structures* 20 (7) (1998) 587–592.
[19] B. Burgart, P. Cartraud, Continuum modeling of beamlike lattice trusses using averaging method, *Computers and Structures* 73 (1999) 267–279.
[20] K. Heki, T. Saka, Stress analysis of lattice plates as anisotropic continuum plates, *Proceedings of the 1971 IASS Pacific Symposium Part II on Tension Structures and Space Frames*, Tokyo and Kyoto, Japan, 1972, pp. 663–674.
[21] H. Tollenaere, D. Caillerie, Continuous modeling of lattice structures by homogenization, *Advances in Engineering Software* 29 (7) (1989) 699–705.
[22] D.L. Dean, R.R. Avent, State of the art of discrete field analysis of space structures, *Proceedings of the Second International Conference on Space Structures*, University of Guildford, England, 1975, pp. 7–16.
[23] T. Wha, Natural frequencies of uniform grillages, *Journal of Applied Mechanics* 30 (1963) 571–578.
[24] T. Wha, Free lateral oscillations of a supported grillage, *Journal of the Franklin Institute* 277 (4) (1964) 349–360.
[25] H.V.S. GangaRao, J.C. Smith, Dynamic field analysis of torsionless grids, *Journal of Engineering Mechanics Division* 98 (3) (1972) 679–693.
[26] Y. Soucy, F.R. Vigneron, Identification of structural properties of a continuous longerons space mast, *Proceedings of the AIAA/ASME/ASCE/AHS 25th Structures, Structural Dynamics and Materials Conference*, Palm Springs, CA, 1984, pp.130–139.
[27] M. Webster, W.V. Velde, Modeling beam-like space trusses with nonlinear joints, *Proceedings of the AIAA/ASME/ASCE/AHS/ASC* 32nd *Structures, Structural Dynamics, and Materials Conference*, Baltimore, MD, 1991, pp. 2745–2754.
[28] J.F. Doyle, Force Identification from dynamic response of a bimaterial beam, *Experimental Mechanics* 33 (1) (1993) 64–69.
[29] D.J. Inman, Modal data extraction, in: *Engineering Vibrations*, third ed., Prentice-Hall, Inc., Upper Saddle River, NJ, 2006, pp. 509–513.